Subspace-constrained deconvolution of auditory evoked potentials

Angel de la Torre,[1, a] Joaquin T. Valderrama,[2, b] Jose C. Segura,[1, c] Isaac M. Alvarez,[1, d] and Jesus Garcia-Miranda[3, e]

[1] *Department of Signal Theory, Telematics, and Communications, University of Granada, Granada, Spain*

[2] *National Acoustic Laboratories, Sydney, Australia*

[3] *Department of Algebra, University of Granada, Granada, Spain*

(Dated: 30 May 2022)

Auditory evoked potentials can be estimated by synchronous averaging when the responses to the individual stimuli are not overlapped. However when the response duration exceeds the inter-stimulus interval, a deconvolution procedure is necessary to obtain the transient response. The iterative randomized stimulation and averaging (IRSA) or the equivalent randomized stimulation with least squares deconvolution (RSLSD) have been proven to be flexible and efficient methods for deconvolving the evoked potentials, with minimum restrictions in the design of stimulation sequences. Recently, a latency-dependent filtering and down-sampling (LDFDS) methodology was proposed for optimal filtering and dimensionality reduction, which is particularly useful when the evoked potentials involve the complete auditory pathway response (i.e. from the cochlea to the auditory cortex). In this case, the number of samples required to accurately represent the evoked potentials can be reduced from several thousands (with conventional sampling) to around 120. In this article we propose to perform the deconvolution in the reduced representation space defined by LDFDS and present the mathematical foundation of the subspace-constrained deconvolution. Under the assumption that the evoked response is appropriately represented in the reduced representation space, the proposed deconvolution provides an optimal least-squares estimation of the evoked response. Additionally, the dimensionality reduction provides a substantial reduction of the computational cost associated to the deconvolution. MATLAB/Octave code implementing the proposed procedures is included as supplementary material.

Keywords: Auditory Evoked Potentials (AEPs); electroencephalogram (EEG); least squares (LS) estimation; iterative randomized stimulation and averaging (IRSA); randomized stimulation with least squares deconvolution (RSLSD); latency-dependent filtering and down-sampling (LDFDS).

[a]Also at: Research Centre for Information and Communications Technologies (CITIC-UGR), University of Granada, Granada, Spain. ORCID: 0000-0002-9736-5190.

[b]Also at: Department of Linguistics, Macquarie University, Sydney, Australia. Electronic mail: joaquin.valderrama@nal.gov.au, joaquin.valderrama@mq.edu.au. ORCID: 0000-0002-5529-8620.

[c]Also at: Research Centre for Information and Communications Technologies (CITIC-UGR), University of Granada, Granada, Spain. ORCID: 0000-0003-3746-0978.

[d]Also at: Research Centre for Information and Communications Technologies (CITIC-UGR), University of Granada, Granada, Spain. ORCID: 0000-0001-5395-4797.

[e]ORCID: 0000-0003-2528-0566.

I. INTRODUCTION

Auditory Evoked Potentials (AEPs) are useful for the study of the auditory system, in the context of hearing research, as well as in the context of clinical practice and diagnosis (Burkard and Don, 2007). AEP recording usually includes the repetition of stimuli and the averaging of the responses in order to improve the signal-to-noise ratio (SNR), usually too low for an isolated response due to the small amplitude of the evoked potentials and the presence of noise (Thornton, 2007).

When stimuli are presented in a repetitive sequence, the standard way for obtaining the response from the electroencephalogram (EEG) is by synchronous averaging the available epochs (Thornton, 2007). However, synchronous averaging implies a restriction: the inter-stimulus interval (ISI) must be longer than the response duration in order to avoid overlapping of sequential responses. For this reason, the recording filters and the response length are conventionally configured according to the AEP components to be recorded: for example, auditory brainstem response (ABR) is recorded in the 100-3000 Hz band with a response duration of around 10 ms; middle latency response (MLR) in the 10-300 Hz band with a response duration of 100 ms; cortical auditory evoked potentials (CAEPs) in the 1-30 Hz band with a response duration of 1 s (Hall, 2007).

Recording AEPs at high stimulation rate, as well as the simultaneously recording of the responses from different portions of the auditory pathway, are relevant for both clinical and research purposes, since they allow the study of neural adaptation mechanisms (Gillespie and Muller, 2009; Thornton and Coleman, 1975; Thornton and Slaven, 1993; Valderrama *et al.*, 2014c), or analyzing the response to complex stimuli more natural than repetitive sequences of clicks (de la Torre *et al.*, 2020; Holt and Ozdamar, 2016; Kohl *et al.*, 2019; Maddox and Lee, 2018; Martinez *et al.*, 2021; Valderrama *et al.*, 2019). However, if the ISI is shorter than the response duration, a deconvolution-based estimation of the AEPs (instead of synchronous averaging) is necessary to disentangle the overlapping responses (Bohorquez and Ozdamar, 2006; Eysholdt and Schreiner, 1982; Valderrama *et al.*, 2014b).

There are different deconvolution-based methods proposed in the literature for recovering AEP responses: maximum length sequences (MLS) (Eysholdt and Schreiner, 1982; Thornton and Slaven, 1993), adjacent-responses (ADJAR) (Woldorff, 1993), quasi-periodic sequence deconvolution (QSD) (Jewett *et al.*, 2004), continuous loop averaging deconvolution (CLAD) (Bohorquez and Ozdamar, 2006; Ozdamar and Bohorquez, 2006), linear deconvolution for baseline correction (LDBC) (Lütkenhöner, 2010), randomized stimulation and averaging (RSA) (Valderrama *et al.*, 2012), iterative randomized stimulation and averaging (IRSA) (de la Torre *et al.*, 2019; Valderrama *et al.*, 2014b, 2016) and randomized stimulation with least-squares deconvolution (RSLSD) (Bardy *et al.*, 2014a,b,c; de la Torre *et al.*, 2019). Among them, IRSA and RSLSD are particularly attractive because of the flexibility they provide for the stimulus design. While some methods require very specific stimulation sequences (like MLS) or a periodical repetition of a pseudo-random stimulation sequence (like CLAD), the IRSA and RSLSD deconvolutions only require the autocorrelation matrix of the stimulation sequence to be invertible (situation usually verified in most practical situations) (Bardy *et al.*, 2014a,c; de la Torre *et al.*, 2019; Valderrama *et al.*, 2014c, 2016). This less restrictive characteristic of IRSA and RSLSD not only provides more flexibility in the experimental design of audiological tests, but also the possibility of designing audiological experiments with more ecologically-valid stimuli (Burkard *et al.*, 2018; de la Torre *et al.*, 2019; Finneran *et al.*, 2019; Martinez *et al.*, 2021; Valderrama *et al.*, 2014c, 2019, 2016).

In a previous study (de la Torre *et al.*, 2019), we demonstrated that the iterative IRSA procedure converges to the RSLSD solution (which supports the mathematical equivalence of IRSA and RSLSD methods) and we proposed a matrix-based implementation of this algorithm providing an efficient computation of the deconvolution of the AEP responses.

More recently, we proposed the application of a latency-dependent filtering and down-sampling (LDFDS) to the AEP responses (de la Torre *et al.*, 2020). This procedure provides an optimal filtering to the evoked responses and also a substantial reduction of the dimensionality required for representing them. LDFDS was reported to be particularly useful for processing the complete auditory pathway response, i.e. including brainstem, middle latency and cortical responses simultaneously. The underlying idea with LDFDS is that each portion of the evoked response involves a specific frequency bandwidth, and therefore an optimal filtering (and also an optimal down-sampling) should change dynamically with the latency, with wider bandwidth and higher sampling-rate at early latency (i.e. in the region of ABR) which progressively decrease as the latency increases (i.e. for the MLR and CAEP components). In this previous article, we demonstrated that LDFDS provides a significant noise reduction thanks to the latency-dependent filtering. Additionally, thanks to the latency-dependent down-sampling, the complete auditory pathway response (including ABR, MLR and CAEP) usually requiring more than 10.000 samples at a constant sampling-rate, can be correctly represented after LDFDS with only 40 samples per decade (a decade is the interval between a latency T and a latency $10 \cdot T$), i.e. with around 120 samples. Therefore, the evoked response can be represented in the original signal representation, or equivalently in a reduced representation, requiring a significantly smaller number of samples (or components) in this last case.

While LDFDS was applied after the deconvolution in our previous work (de la Torre *et al.*, 2020), in the current work we propose to perform the deconvolution (either with IRSA or with RSLSD) in the reduced representation given by LDFDS, i.e. we propose a deconvolution constrained to the subspace defined by LDFDS. This proposal implies two important differences. On one hand, as we discuss in the present work, the subspace-constrained deconvolution provides an optimal least squares estimation of the evoked response. On the other hand, since the IRSA algorithm involves iterative matrix products and RSLSD involves a matrix division, a substantial reduction of the problem dimensionality (typically from several thousands to around 100 or 200 dimensions) implies a substantial reduction of the computational cost in both deconvolution algorithms.

In this work we present the mathematical foundation of the LDFDS-based subspace-constrained least squares (SC-LS) deconvolution as an optimal solution when the evoked response is assumed to be contained in the associated subspace (i.e. properly represented with LDFDS). We also discuss the quality of the proposed estimation (in terms of the expected energy of the estimation error), as well as the computational cost. The experimental results, including both simulations and estimation of real AEP responses, illustrate the utility of the proposed subspace-constrained deconvolution for recording AEPs including the response of the complete auditory pathway.

II. SUBSPACE-CONSTRAINED DECONVOLUTION

A. Least squares deconvolution

In an AEP recording procedure, the EEG is usually modeled as a convolutional process (Jewett *et al.*, 2004; Ozdamar and Bohorquez, 2006):

$$y(n) = s(n) * x(n) + n_0(n) \tag{1}$$

where $y(n)$, $s(n)$ and $n_0(n)$ are digital signals representing, respectively, the EEG, the stimulation sequence (consisting of one impulse at the beginning of each stimulation event), and the noise affecting the EEG; n is the index for the samples ($n \in \{0, \ldots, N-1\}$, being N the number of samples of the EEG); $x(n)$ represents the response evoked by each stimulus (with $x(n)$ null for $n > (J-1)$, being J the length of the evoked response); and the asterisk ($*$) represents discrete time convolution.

This convolutional model can be rewritten using a matrix notation (de la Torre *et al.*, 2019):

$$\mathbf{y} = S\mathbf{x} + \mathbf{n}_0 \tag{2}$$

where $\mathbf{y}$, $S\mathbf{x}$ and $\mathbf{n}_0$ are N-component column vectors (representing the EEG signal, the convolution of the stimulation signal with the response and the noise, respectively), $\mathbf{x}$ is a J-component column vector representing the evoked response and S is a $(N \times J)$ matrix (with N rows and J columns) with $S(n, j) = s(n-j)$ providing the convolution $s(n) * x(n)$ as a matrix operation.

The deconvolution of $\mathbf{y}$, i.e. the estimation of the response $\mathbf{x}$, can be formulated either as an over-determined system of linear equations (with N equations and J unknowns, being

$N \gg J$), in the context of linear algebra, or as a multiple linear regression problem, in the context of statistics (Gentle, 1998; Goldberger *et al.*, 1964; Hayashi, 2000; Lawson and Hanson, 1974). Assuming linearity and uncorrelated-stationary-white noise (i.e. if linearity, exogeneity and homocedasticity conditions are verified) the ordinary least squares (LS) solution provides a minimum-variance unbiased estimation of the response (Hayashi, 2000). The LS criterion minimizes the sum of the squared residuals, or equivalently the squared distance between the EEG and the expected convolution:

$$\hat{\mathbf{x}}_{LS} = \arg\min_{\mathbf{x}} \|\mathbf{y} - S\mathbf{x}\|^2 \tag{3}$$

and the solution derived from this criterion, i.e. the LS deconvolution, is (Gentle, 1998; Hayashi, 2000; Press *et al.*, 2002):

$$\hat{\mathbf{x}}_{LS} = \left(S^T S\right)^{-1} S^T \mathbf{y} \tag{4}$$

where S^T is the transpose of S.

By defining the matrix S_k as the normalized and transposed of S, (i.e. $S_k = S^T/K$, where K is the number of impulses in the stimulation sequence), and taking into account that $R_s = S_k\, S$ is the normalized $(J \times J)$ autocorrelation matrix of the stimulation sequence $s(n)$, the LS deconvolution can be rewritten as:

$$\hat{\mathbf{x}}_{LS} = R_s^{-1}\, S_k\, \mathbf{y} = R_s^{-1}\, \mathbf{z}_0 \tag{5}$$

where $\mathbf{z}_0 = S_k\, \mathbf{y}$ is a J-component vector obtained as the synchronous averaging of the EEG. The derivation of the LS estimation is detailed in section 1 of the supplementary materials[1].

The LS estimation of the evoked response, requires the synchronous averaging of the EEG ($\mathbf{z}_0$) and the inversion of the $(J \times J)$ normalized autocorrelation matrix of the stimulation sequence (R_s^{-1}). This LS estimation can be obtained by matrix division (as proposed in RSLSD (Bardy *et al.*, 2014a,b,c)). Alternatively the IRSA procedure (de la Torre *et al.*, 2019) proposes an iterative LS estimation of the response according to the following recursion:

$$\hat{\mathbf{x}}_i = \hat{\mathbf{x}}_{i-1} + \alpha \mathbf{z}_{i-1} \tag{6}$$

$$\mathbf{z}_i = \mathbf{z}_0 - R_s \hat{\mathbf{x}}_i \tag{7}$$

where α is a convergence parameter that must be small enough ($\alpha < 2/\max \lambda_i$, being λ_i the eigenvalues of R_s) in order to guarantee the stability of the algorithm.

B. Latency-dependent filtering and down-sampling

Since each portion of the evoked response requires a specific bandwidth (range 100-3000 Hz for ABR; 10-300 Hz for MLR; 1-30 Hz for CAEPs) a latency dependent filtering was proposed by (de la Torre *et al.*, 2020) for optimally filtering the AEP responses. The latency-dependent filtering is implemented as a matrix operator, where the impulsive response changes from row to row, in order to adapt to the bandwidth required at each latency (lower cut-off frequency as the latency increases). Moreover, since the bandwidth changes with the latency, according to the sampling theorem, the sampling rate can also be adapted to optimal values at each specific latency. The latency-dependent down-sampling can easily be implemented by appropriately selecting specific rows of the latency-dependent filtering matrix.

This way, the latency-dependent filtering and down-sampling (LDFDS) is implemented by means of a ($J_r \times J$) matrix V_r, with J being the dimensionality of the representation space of the original AEP response and J_r that of the reduced representation space (i.e. after the filtering and down-sampling). The reduced representation (with J_r components) of the LS deconvolution is obtained by multiplying the LDFDS matrix V_r and the J-component original vector $\hat{\mathbf{x}}_{LS}$ (representing the LS estimation of the AEP response):

$$(\hat{\mathbf{x}}_{LS})_r = V_r\,\hat{\mathbf{x}}_{LS} \tag{8}$$

With the proposed procedure, the noise out of the frequency bands of interest is efficiently removed, and the dimensionality is reduced typically from several thousands of samples to 40 samples per decade (around 120 samples for accurately representing the complete auditory pathway response). Additionally, the rows of the LDFDS matrix are orthonormalized, which preserves the metrics (i.e. the distances and energies) in the reduced representation space. The orthonormality of the rows allows the recovery of the optimally latency-dependent filtered response in the original representation (at the original sampling rate and with J components), $\hat{\mathbf{x}}_{ldf}$, by multiplying the reduced representation and the transpose of the LDFDS matrix:

$$\hat{\mathbf{x}}_{ldf} = V_r^T\,(\hat{\mathbf{x}}_{LS})_r \tag{9}$$

C. Subspace-constrained least squares deconvolution

If we assume that the response to be estimated $\mathbf{x}$ is appropriately represented with the reduced representation $\mathbf{x}_r$ given by V_r, (or equivalently, if the latency-dependent filtering provided by V_r is appropriate for the evoked response $\mathbf{x}$), then we can write:

$$\mathbf{x} = \mathbf{x}_{ldf} = V_r^T\,\mathbf{x}_r \tag{10}$$

and the convolutional model provided in equation (2) can be rewritten as:

$$\mathbf{y} = S\,V_r^T\,\mathbf{x}_r + \mathbf{n}_0 \tag{11}$$

This equation is mathematically similar to equation (2), with the following differences: (i) the unknowns is the J_r-component vector $\mathbf{x}_r$, instead of the J-component vector $\mathbf{x}$; and (ii) it involves the $(N \times J_r)$ matrix $(S\,V_r^T)$, instead of the $(N \times J)$ matrix S. The equation (11) can be again formulated as another over-determined system of linear equations, or as a multiple linear regression problem, with the difference of the significant dimensionality reduction provided by LDFDS. This dimensionality reduction implies that the convolution problem is constrained to the subspace associated to the matrix V_r, or equivalently, the solution of the system of equations is forced to be in the subspace of responses compatible with the latency dependent filtering, with J_r freedom degrees (instead of J). The formal LS solution is similar to that in equation (4), but using $(S\,V_r^T)$ instead of S:

$$\begin{aligned}
\hat{\mathbf{x}}_{rLS} &= \left((S\,V_r^T)^T(S\,V_r^T)\right)^{-1}\,(S\,V_r^T)^T\,\mathbf{y} = \\
&= \left(V_r\,S^T\,S\,V_r^T\right)^{-1}\,V_r\,S^T\,\mathbf{y} = \\
&= \left(V_r\,R_s\,V_r^T\right)^{-1}\,V_r\,S_k\,\mathbf{y} = \\
&= \left(V_r\,R_s\,V_r^T\right)^{-1}\,V_r\,\mathbf{z}_0 = R_{s\,r}^{-1}\,\mathbf{z}_{0\,r}
\end{aligned} \tag{12}$$

where $R_{s\,r}$ and $\mathbf{z}_{0\,r}$ are, respectively, R_s and $\mathbf{z}_0$ projected into the subspace. According to this equation, the subspace-constrained LS deconvolution of the EEG can be obtained with the following steps: (i) the autocorrelation matrix R_s and the synchronous averaging of the EEG $\mathbf{z}_0$ must be transformed to the subspace using the transformation V_r; (ii) the autocorrelation matrix in the reduced representation must be inverted; and (iii) the inverted reduced autocorrelation matrix must be applied to the reduced synchronous averaging. As can be observed, the LS deconvolution in (12) is similar to that in equation (5), with the difference that the problem is solved in the reduced representation space.

Since it is assumed that the LS solution is contained in the subspace defined by V_r, this procedure requires that the evoked response is correctly described in this subspace. Otherwise, the procedure will provide a biased solution, as discussed in the section 2 of the supplementary materials[1].

Interestingly, since the matrix to be inverted has a size $(J_r \times J_r)$ instead of $(J \times J)$, the subspace-constrained deconvolution provides a substantial reduction of the computational load. Moreover, since the solution is expected to be contained in the subspace, the subspace constrain and the LS criterion guarantee that the $\hat{\mathbf{x}}_{rLS}$ solution is closer to the evoked response $\mathbf{x}$ than the non-constrained solution $\hat{\mathbf{x}}_{LS}$.

As in the case of the original representation space, the subspace-constrained LS deconvolution can be implemented with matrix division as proposed for RSLSD. Alternatively, it can be implemented with the IRSA recursion constrained to the subspace, i.e. using $R_{s\,r}$ and $\mathbf{z}_{0\,r}$ instead of R_s and $\mathbf{z}_0$ in equations (6) and (7):

$$\hat{\mathbf{x}}_{i\,r} = \hat{\mathbf{x}}_{i-1\,r} + \alpha \mathbf{z}_{i-1\,r} \tag{13}$$

$$\mathbf{z}_{i\,r} = \mathbf{z}_{0\,r} - R_{s\,r}\,\hat{\mathbf{x}}_{i\,r} \tag{14}$$

and the demonstration of the IRSA convergence to the LS solution is similar in both the original and the reduced representation space.

D. Energy of the error in the estimated response

Taking into account equations (2) and (5) we can write:

$$\hat{\mathbf{x}}_{LS} = R_s^{-1}\, S_k\, \mathbf{y} = R_s^{-1}\, S_k (S\, \mathbf{x} - \mathbf{n}_0) =$$
$$= R_s^{-1}\, R_s\, \mathbf{x} + R_s^{-1}\, S_k\, \mathbf{n}_0 =$$
$$= \mathbf{x} + R_s^{-1}\, S_k\, \mathbf{n}_0 \tag{15}$$

and the error of the LS estimation is:

$$\mathbf{e}_{LS} = \hat{\mathbf{x}}_{LS} - \mathbf{x} = R_s^{-1}\, S_k\, \mathbf{n}_0 = R_s^{-1}\, \mathbf{n}_A \tag{16}$$

where $\mathbf{n}_A = S_k \mathbf{n}_0$ is the synchronous averaging of the noise affecting the EEG. The noise affecting the EEG is unknown, and therefore the error affecting the estimated evoked potential cannot be calculated. However, taking into account the statistics of the noise (described with its covariance matrix Σ_{n_0}) and the previous equation, we can calculate the covariance matrix $\Sigma_{e_{LS}}$ of the error affecting the estimated response (whose trace is the expected energy of the error):

$$\Sigma_{e_{LS}} = R_s^{-1}\, S_k\, \Sigma_{n_0}\, S_k^T\, (R_s^{-1})^T = R_s^{-1}\, \Sigma_{n_A}\, R_s^{-1} \tag{17}$$

where Σ_{n_A} is the $(J \times J)$ covariance matrix of the noise after the synchronous averaging (which is a positive semidefinite, Toeplitz and symmetric matrix, as Σ_{n_0}), and the fact that R_s (as well as its inverse) is symmetric has also been taken into account.

A similar derivation can be done when the LS deconvolution is performed in the reduced representation space. In such case, the error affecting the LS estimation in the reduced representation space is:

$$\mathbf{e}_{rLS} = \hat{\mathbf{x}}_{rLS} - \mathbf{x}_r = (V_r\, R_s\, V_r^T)^{-1}\, V_r\, \mathbf{n}_A \tag{18}$$

and the corresponding covariance matrix is:

$$\Sigma_{e_{rLS}} = (V_r\, R_s\, V_r^T)^{-1}\, V_r\, \Sigma_{n_A}\, V_r^T (V_r\, R_s\, V_r^T)^{-1} \tag{19}$$

where both the reduced autocorrelation matrix $(V_r\, R_s\, V_r^T)$ and its inverse are symmetric.

The LS criterion guarantees that the LS solution is optimal (in the sense that provides an unbiased and minimum variance estimation of $\mathbf{x}_r$, under the required assumptions) and therefore, if the response is expected to be contained in the subspace defined by V_r, the energy of the error (as well as the variance of the estimation) is expected to be smaller when the LS solution is constrained to this subspace. Under the LS assumptions (including uncorrelated and stationary white noise) it is easy to demonstrate that the energy of the error decreases, or equivalently that the trace of the covariance matrix of the error decreases:

$$\mathrm{tr}(\Sigma_{e_{rLS}}) < \mathrm{tr}(\Sigma_{e_{LS}}) \tag{20}$$

The demonstration is included in the section 3 of the supplementary materials[1].

E. Comparison of subspace-constrained deconvolution vs. LDFDS after deconvolution

The LS criterion guarantees that $\hat{\mathbf{x}}_{rLS}$ is an optimal solution under several assumptions: $\mathbf{x}$ is in the subspace, $s(n)$ and $n_0(n)$ are uncorrelated and $n_0(n)$ is stationary-white noise.

We have verified that the energy of the expected error for $\hat{\mathbf{x}}_{rLS}$ is less than or equal to that for $\hat{\mathbf{x}}_{LS}$. However, when LDFDS was proposed, $\hat{\mathbf{x}}_{LS}$ was first estimated and then projected into the subspace:

$$(\hat{\mathbf{x}}_{LS})_r = V_r\,\hat{\mathbf{x}}_{LS} = V_r\,R_s^{-1}\,\mathbf{z}_0 \tag{21}$$

and it was demonstrated to be effective for noise reduction (i.e., $(\hat{\mathbf{x}}_{LS})_r$ substantially improves $\hat{\mathbf{x}}_{LS}$). Therefore, one could wonder whether the subspace-constrained deconvolution $\hat{\mathbf{x}}_{rLS}$ proposed here improves or not the estimation obtained when LDFDS is applied after a non constrained deconvolution $(\hat{\mathbf{x}}_{LS})_r$, previously proposed in (de la Torre *et al.*, 2020).

Of course, under the required assumptions, the LS criterion guarantees that the subspace-constrained deconvolution is better, but some analysis is also interesting. Both approaches can be compared taking into account the trace of the covariance matrix of the error affecting the corresponding estimations. The covariance matrix of the error is given in equation (19) for $\hat{\mathbf{x}}_{rLS}$. In the case of $(\hat{\mathbf{x}}_{LS})_r$, the covariance matrix of the error is:

$$\Sigma_{(e_{LS})_r} = V_r R_s^{-1} \Sigma_{nA} R_s^{-1} V_r^T \tag{22}$$

In the section 4 of the supplementary materials[1], the traces of both covariance matrices are compared. As expected, under the assumptions (particularly, in the case of white noise), it is demonstrated that the trace for the subspace-constrained deconvolution is less than or equal to that for $(\hat{\mathbf{x}}_{LS})_r$:

$$\mathrm{tr}(\Sigma_{e_{rLS}}) \leq \mathrm{tr}(\Sigma_{(e_{LS})_r}) \tag{23}$$

Interestingly, the equality occurs if $R_s = I$. This situation never takes place in a deconvolution problem (because if $R_s = I$ then the optimal solution is obtained with the synchronous averaging). However R_s is usually relatively close to the identity matrix, and therefore the solutions $(\hat{\mathbf{x}}_{LS})_r$ and $\hat{\mathbf{x}}_{rLS}$ are expected to be close.

III. EXPERIMENTS AND RESULTS

The experiments have been designed to compare (i) the LS solution (ii) the LS solution transformed to the reduced subspace and (iii) the subspace-constrained LS solution, corresponding to the estimations $\hat{\mathbf{x}}_{LS}$, $(\hat{\mathbf{x}}_{LS})_r$ and $\hat{\mathbf{x}}_{rLS}$, and referred to as LS, LS-R and SC-LS, respectively. These are compared in terms of both the quality of the estimated responses and the computational cost of the procedures. According to the RSLSD and IRSA procedures, we have compared implementations based on both matrix division ($\mathrm{LS}_{\mathrm{MD}}$, $\mathrm{LS\text{-}R}_{\mathrm{MD}}$ and $\mathrm{SC\text{-}LS}_{\mathrm{MD}}$) and iterative estimation ($\mathrm{LS}_{\mathrm{It}}$, $\mathrm{LS\text{-}R}_{\mathrm{It}}$ and $\mathrm{SC\text{-}LS}_{\mathrm{It}}$).

The quality evaluation of the estimated responses requires an a-priori knowledge of the clean signal, to be used as reference, which is not possible with real AEP responses (because the estimations are always affected by some residual noise). Therefore, the quality evaluations are based on simulations (where a noisy EEG can be synthesized using a known clean AEP response, which can be used as reference). The evaluation of the computational cost is based on real EEG signals.

A. Experimental design

For the experiments involving real EEG signals, the stimulation consisted in rarefaction clicks of 0.1 ms at 74 dB normal hearing level (nHL) presented at different average stimulation rates, between 1.39 and 44.44 stimuli per second (stim/sec). The 0 dB nHL reference level was estimated as described in Martinez *et al.* (2022), i.e. as the mean threshold level estimated in a sample of 10 normal-hearing adults (5 female, 23-38 years) who presented pure-tone threshold levels within the normal range in the 0.5-8 kHz frequency range and had no history of any type of auditory dysfunction. At each average stimulation rate, the ISI has a uniform distribution within one octave of variation (e.g. 480-960 ms for average stimulation rate of 1.39 stim/sec; 240-480 ms for 2.78 stim/sec; etc.). Six stimulation conditions are considered, with one octave of variation from condition to condition (i.e. double average stimulation rate and half ISI-limits for the next condition). The EEGs were recorded with surface electrodes located at the forehead (active), right mastoid (reference) and middle forehead (ground) using a preamplifier with 70 dB gain and 1-3500 Hz bandwidth (Valderrama *et al.*, 2013, 2014a,c). The preamplified EEG signal was digitized (44100 Hz, 16 bits/sample) low-pass filtered (4000 Hz cut-off frequency) and down-sampled to 14700 Hz. Eye-blinking artifacts were suppressed with the iterative template matching and suppression algorithm (ITMS) (Valderrama *et al.*, 2018). The EEG database (previously used in de la Torre *et al.* (2020)) contains recordings from 8 subjects (aged 26-58 yr., one female) with 6 ISI conditions for each subject, and 684 seconds of EEG recording for each ISI condition. All the participants of this database met the inclusion criteria of reporting no hearing difficulties and absence of a history of auditory dysfunction. In order to obtain the response of the complete auditory pathway, the AEP response extends from 0 to 1000 ms, i.e. the response length is $J = 14700$ samples. The latency-dependent filtering and down-sampling is performed with a resolution of 40 samples/decade, which provides a response length in the reduced representation space of $J_r = 117$ samples.

The experiments involving simulations are designed with a configuration similar to that of the real experiments (same ISI conditions and EEG duration). The grand-average AEP responses obtained in (de la Torre *et al.*, 2020) at each ISI condition were used as reference clean AEP responses in order to synthesize the simulated EEGs. These reference AEP responses were latency-dependent filtered with a resolution of 40 samples/decade. The EEGs are synthesized according to the convolutional model in equation (1). The noise contaminating the EEGs was band-pass random noise (with flat spectral density in the range [1.5-800] Hz and ± 20 dB/decade slope out of the pass-band). It was prepared from white Gaussian noise, filtered with a first-order 1.5-800 Hz Butterworth band-pass filter. The noise level was adjusted in order to obtain a final SNR (after the standard LS deconvolution) around +10 dB, which is a reasonable SNR for typical AEP estimations (de la Torre *et al.*, 2020).

In the simulation-based experiments, the AEP response $\hat{\mathbf{x}}$ is estimated from the EEG $\mathbf{y}$ either with the LS, LS-R or SC-LS procedures. Using the clean reference $\mathbf{x}$, the error can be estimated as $\mathbf{e} = \hat{\mathbf{x}} - \mathbf{x}$, and the different procedures can easily be compared in terms of the error energy. However, since the noise affecting the EEG is a random process the error energy estimations are strongly affected by statistical fluctuations. For this reason, the three procedures have been compared in terms of the expected error energy (statistically consistent with the measured error energies but more stable than them) using the trace of the covariance matrix of the respective errors, in equations (17), (22) and (19) for LS, LS-R and SC-LS, respectively. The simulations have been repeated 100 times for each ISI condition, and expected error measurements have been averaged.

For the experiments involving real EEGs and evaluation of the computational cost, the LS, LS-R and SC-LS estimations have been obtained with algorithms based on both, RSLSD (i.e. involving matrix division) and IRSA (i.e. involving iterative estimation). MatLab/Octave functions implementing the RSLSD and IRSA algorithms for LS, LS-R and SC-LS estimations are described in the section 5 of the supplementary materials[1], together with a demonstration script providing a simulation and examples of use of these functions. The convergence criterion for the iterative estimations was set either to 290 dB (more accurate) or to 120 dB (faster). The computational cost was evaluated in terms of execution time, measured using a desktop computer with an Intel-Core i7-3770 CPU, 3.40 GHz, 8.00 GB RAM running the algorithms with MatLab.

B. Quality of the LS, LS-R and SC-LS estimations

Figure 1 represents an example the AEP responses obtained in the simulations for one of the 100 repetitions. The figure includes the clean AEP responses used for the EEG synthesis (and as reference for the quality estimations), and the different estimations based on LS, LS-R and SC-LS (with the matrix division implementation). The six responses in each panel correspond to the different ISI conditions considered in the simulations, from 480-960 ms (top) to 15-30 ms (bottom). The latency axis is logarithmically scaled in order to appropriately represent the response of the complete auditory pathway, from the auditory brainstem responses to the cortical responses. The main waves of the AEP response are labeled, and the stimulation artifact can be observed within the first ms. As can be observed, the LS estimation is strongly affected by noise (due to the noise added to the EEG). The

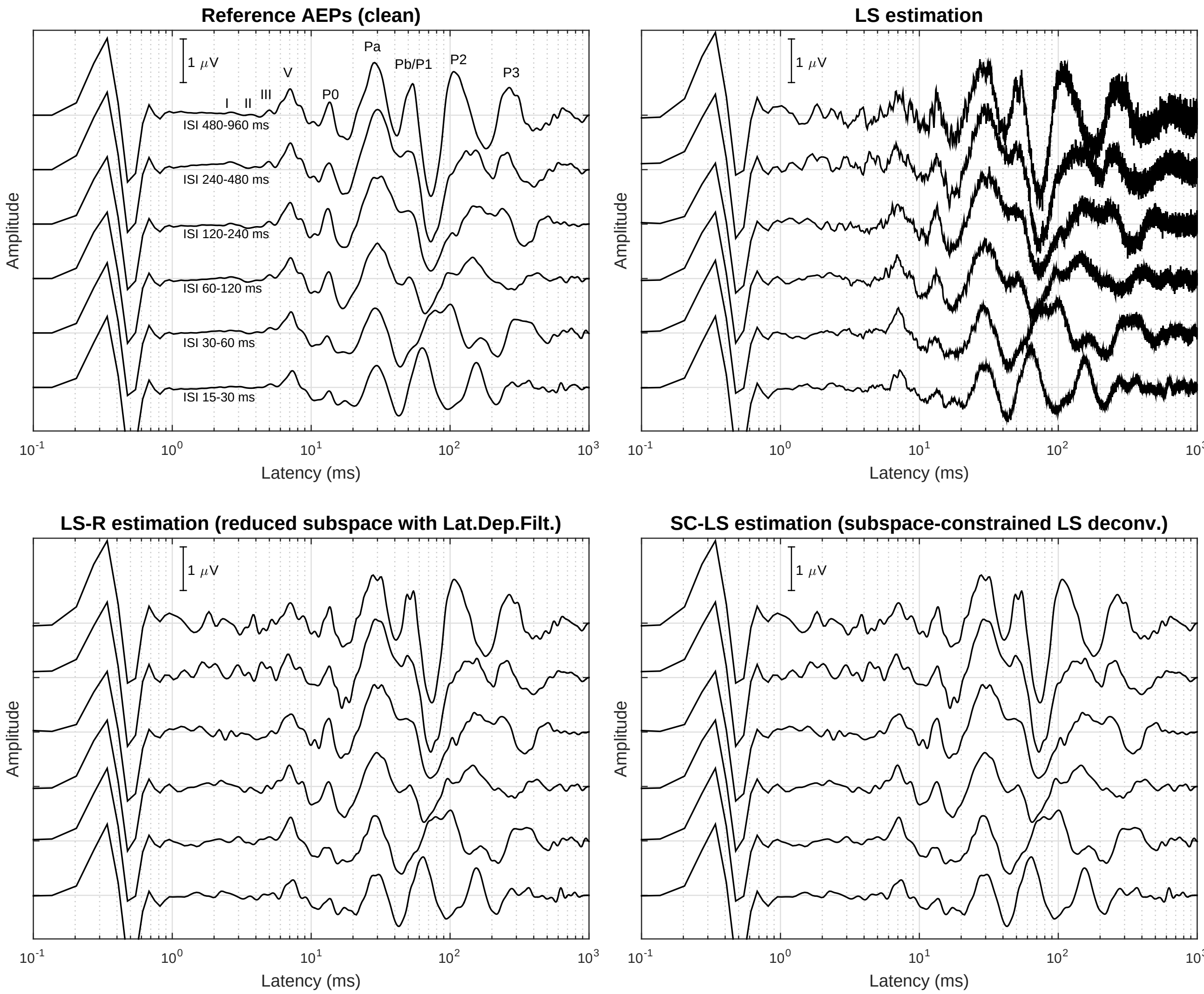

FIG. 1. AEP responses obtained in the simulations for one repetition. The different panels represent (a) the template responses used as reference; (b) the LS estimations (obtained in the original representation space); (c) the LS-R estimations (obtained by applying dimensionality reduction based on the LDFDS to the LS estimations); and (d) the SC-LS estimations (subspace-constrained LS deconvolution). The plots in each panel correspond to the AEP responses at each ISI condition.

TABLE I. SNR mean (standard deviation in parenthesis) in dB, for the LS, LS-R and SC-LS estimations, obtained in simulations with 100 repetitions for each ISI condition. The SNR measurements are based on the covariance matrix of the error.

ISI condition	LS mean (std) dB	LS-R mean (std) dB	SC-LS mean (std) dB
480-960 ms	9.351 (0.002)	23.181 (0.014)	23.188 (0.014)
240-480 ms	9.252 (0.012)	22.672 (0.023)	22.686 (0.023)
120-240 ms	9.589 (0.008)	21.778 (0.035)	21.810 (0.035)
60-120 ms	7.614 (0.004)	17.645 (0.041)	17.688 (0.041)
30-60 ms	11.472 (0.008)	19.180 (0.045)	19.209 (0.045)
15-30 ms	11.610 (0.008)	17.928 (0.030)	17.948 (0.030)
Average	9.815 (1.379)	20.397 (2.238)	20.421 (2.230)

LS-R and SC-LS estimations are significantly less affected by noise. Interestingly, the LS-R and SC-LS estimations are very similar. The comparison of the different estimations is detailed in the section 6.1 of the supplementary materials[1].

The quality of each estimation has been evaluated using the expected SNR, defined as the ratio of the signal energy to the expected error energy, expressed in dB, where the expected error energy was estimated as the trace of the covariance matrix of the residual error:

$$\mathrm{SNR}_{\mathrm{dB}} = 10\log_{10}\left(\frac{E(\mathbf{x})}{E(\mathbf{e})}\right) \approx 10\log_{10}\left(\frac{E(\mathbf{x})}{\mathrm{tr}(\Sigma_e)}\right) \tag{24}$$

The supplementary materials[1] include, in section 6.2, a description of the autocorrelation functions of the noise and the averaged noise (providing Σ_{n_0} and Σ_{n_A}, respectively) and the main diagonal of the covariance matrix of the residual error for the LS, LS-R and SC-LS estimations.

Table I shows the expected SNR obtained for the LS, LS-R and SC-LS estimations, based on the respective covariance matrices. The table includes means and standard deviations

TABLE II. SNR improvement provided by LS-R with respect to LS and by SC-LS with respect to LS-R, in dB, obtained in simulations with 100 repetitions for each ISI condition. The SNR measurements are based on the trace of the covariance matrix of the error. The table includes mean, standard deviation and the p parameter for a paired Student's t-test.

	LS-R vs. LS		SC-LS vs. LS-R	
ISI cond.	mean (std) dB	p	mean (std) dB	p
480-960 ms	13.830 (0.013)	1.4e-300	0.006 (4.4e-4)	4.0e-117
240-480 ms	13.419 (0.018)	2.0e-287	0.014 (8.1e-4)	3.8e-124
120-240 ms	12.188 (0.038)	6.1e-250	0.033 (1.1e-3)	1.2e-149
60-120 ms	10.031 (0.037)	2.1e-242	0.043 (4.9e-4)	6.2e-194
30-60 ms	7.708 (0.040)	9.2e-228	0.028 (5.6e-4)	4.5e-171
15-30 ms	6.318 (0.023)	2.7e-244	0.020 (4.2e-4)	4.0e-168
Average	10.582 (2.830)	<1e-320	0.024 (0.012)	7.5e-211

(SD) for each ISI condition. As can be observed (and consistently with the example in figure 1) there is a substantial improvement in LS-R and SC-LS with respect to LS (associated to the latency dependent filtering), and a very slight improvement of SC-LS with respect to LS-R (associated to the LS resolution constrained to the subspace). Table II evaluates the improvement of LS-R with respect to LS and that of SC-LS with respect to LS-R, including the mean and standard deviation of the SNR difference and the p value of a paired Student's t-test (i.e. the probability of the null hypothesis of statistical independence). The improvement associated to the latency dependent filtering is between 6.3 and 13.8 dB, depending on the ISI condition, which is consistent with the results reported in (de la Torre *et al.*, 2020). The subspace-constrained deconvolution provides a moderate (but systematic) improvement, between 0.006 and 0.043 dB depending on the ISI condition.

TABLE III. Mean execution time across subjects for different ISI conditions in the experiments with real EEGs. The columns correspond to the different deconvolution algorithms. The rows correspond to the different ISI conditions. The last row represents the execution time for processing the six ISI conditions.

ISI (ms)	LS_{MD} (RSLSD)	LS_{It} (IRSA-290dB)	LS_{It} (IRSA-120dB)	$LS\text{-}R_{MD}$ (RSLSD)	$LS\text{-}R_{It}$ (IRSA-290dB)	$LS\text{-}R_{It}$ (IRSA-120dB)	$SC\text{-}LS_{MD}$ (RSLSD)	$SC\text{-}LS_{It}$ (IRSA-290dB)	$SC\text{-}LS_{It}$ (IRSA-120dB)
480-960	20.23 s	0.63 s	0.55 s	20.50 s	0.61 s	0.53 s	0.59 s	0.59 s	0.59 s
240-480	20.91 s	1.79 s	1.09 s	20.74 s	1.75 s	1.09 s	1.01 s	1.03 s	1.02 s
120-240	21.58 s	3.75 s	2.03 s	21.34 s	3.71 s	2.01 s	1.74 s	1.77 s	1.75 s
60-120	22.10 s	7.05 s	3.60 s	22.18 s	6.99 s	3.65 s	2.47 s	2.52 s	2.49 s
30-60	22.99 s	13.48 s	6.66 s	22.99 s	13.47 s	6.63 s	3.52 s	3.65 s	3.59 s
15-30	25.87 s	17.16 s	13.05 s	25.82 s	17.00 s	12.97s	6.31 s	6.42 s	6.32 s
All	**133.69 s**	**43.86 s**	**26.98 s**	**133.58 s**	**43.53 s**	**26.88 s**	**15.63 s**	**15.98 s**	**15.76 s**

These improvements are statistically significant, as can be appreciated from the p values in table II.

The supplementary materials[1] include, in section 6.3, results of the SNRs estimated from the error observed at each repetition of the simulation. The SNRs obtained from the expected error and from the observed error are statistically consistent (same mean values) even though the standard deviations are much greater for the SNRs derived from the observed error (due to statistical fluctuations).

C. Computational cost of the procedures

The computational cost of the deconvolution procedures is compared in table III. The three deconvolution procedures (LS, LS-R, SC-LS) have been implemented with matrix division (using the RSLSD algorithm) and with the iterative estimation (using the IRSA algorithm with convergence criterion of either 290 dB or 120 dB). The table includes the execution time for each ISI condition (average execution time per subject). The last row represents the execution time for the complete test (including the six ISI conditions). The results for LS and LS-R (with similar execution times) reveals that the computational cost of the latency dependent filtering is very small compared with that of the deconvolution. However, the SC-LS provides a significant reduction of the execution time with respect to LS or LS-R, thanks to the dimensionality reduction (from $J = 14700$ to $J_r = 117$). While the IRSA procedure provides a relevant computational cost reduction with respect to RSLSD in the case of LS and LS-R, when the deconvolution is constrained to the subspace the computational costs are very similar. The section 7.1 of the supplementary materials[1] provides more details about the execution times (including initialization and time devoted to each iteration). It also provides a comparison of the execution times measured with a faster computer.

The execution times reported in table III correspond to a response length of 14700 samples. In order to evaluate the influence of the response length over the computational cost, the execution time has been evaluated for J ranging between 14700 (1000 ms) and 147 (10 ms). Figure 2 represents the total execution time per subject as a function of the response length, for the LS-R and SC-LS deconvolution algorithms (LS has not been included in the plot, since it provides execution times similar to those of LS-R). As can be observed, the execution time decreases with the response length, and the improvements are less important as J decreases (because the ratio J/J_r decreases with J).

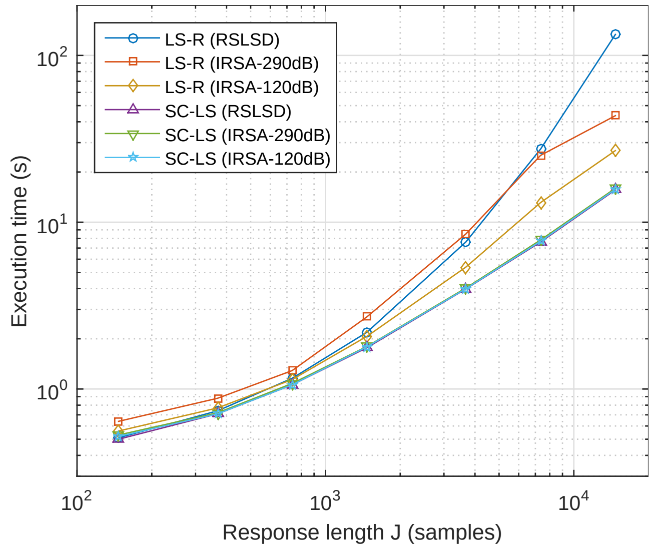

FIG. 2. Mean execution time across subjects required by the different algorithms for processing all the ISI conditions, as a function of the response length J.

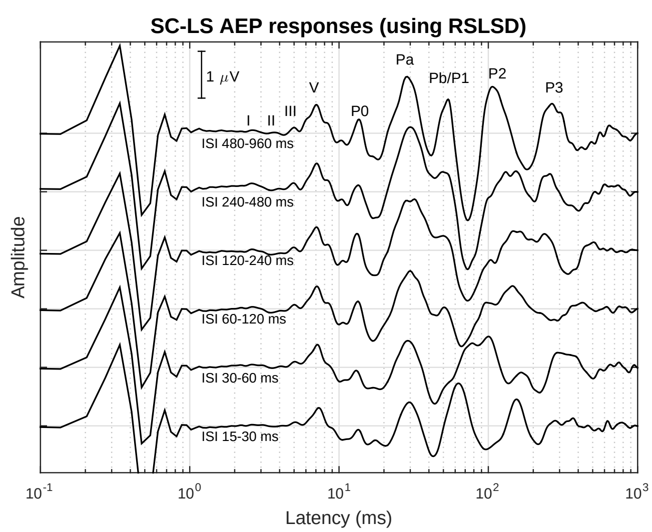

FIG. 3. Grand-average responses obtained with SC-LS$_{\mathrm{MD}}$ for the experiments using real EEG signals.

D. Responses provided by the SC-LS deconvolution

Figure 3 represents the grand-average of the AEP responses provided by the subspace-constrained least squares deconvolution. These responses correspond to the solutions provided by the SC-LS_{MD} algorithm (i.e. SC-LS criterion implemented with matrix division). As in the figure 1, the latency axis is logarithmically scaled, in order to represent the responses of the different portions of the auditory pathway. This responses are very similar to those obtained in (de la Torre *et al.*, 2020), and represented in the upper-left panel of figure 1, because they have been obtained from the same EEG database and also because the solutions provided by LS-R (i.e. applying the latency-dependent filtering) and SC-LS are very similar (the energy of the difference between both solutions is about 31 dB below the signal energy in these experiments). Section 7.2 of the supplementary materials[1] evaluates the differences among the solutions provided by the different deconvolution algorithms considered in this manuscript.

E. Grand-average and individual AEP responses

Figure 4 shows, in the top-left panel, the grand-average AEP responses across participants obtained with SC-LS_{MD} at different stimulation rates. The rest of the panels show the individual responses for each participant. The AEP components are labeled in the grand-average response presented at the top (corresponding to ISI 480-960 ms). The latency has been limited in these plots to the range [1-1000] ms in order to ease the analysis of the evoked response (detailed individual responses including also the stimulation artifact portion can be found in the Section 7.3 of the supplementary materials[1]).

The plots with individual traces (subjects 1 to 8) visually show that all the AEP components from wave I of the ABR to the P3 can be identified in all subjects at the slow presentation rate. Overall, the amplitude of the components decreases as the stimulus rate increases. Moreover, the grand-average AEP responses presented in Panel A, and the individual subplots show that the components from wave I to Pa are highly reproducible, and that they can be tracked from the slow to the faster presentation rates. However, the P1/Pb, P2 and P3 components present a higher variability as rate increases, and they are more difficult to be tracked from the slow to the faster rates.

In addition, subject 7 presents a post-auricular muscle response (PAMR) in all the AEP traces (an action potential occurring at approximately 13 ms after the stimulus onset resulting from the contraction of a muscle located behind the ear, i.e. the post-auricular muscle). The amplitude of the PAMR decreases as the stimulus rate increases. A remarkable negative peak at the latency corresponding to N1 (between Pb/P1 and P2) is also observed for this subject at slow presentation rates. The Section 7.3 of the supplementary materials[1] includes a comparison of the grand-average responses including and excluding this particular subject (when subject 7 is excluded, the morphology of the grand-average responses is quite similar, except for the amplitude reduction in waves P0 and N1).

IV. DISCUSSION AND CONCLUSIONS

In this work we propose the subspace-constrained LS deconvolution for the estimation of the AEPs, based on the LDFDS dimensionality reduction. The manuscript presents the mathematical foundation of the subspace-constrained deconvolution, a theoretical analysis

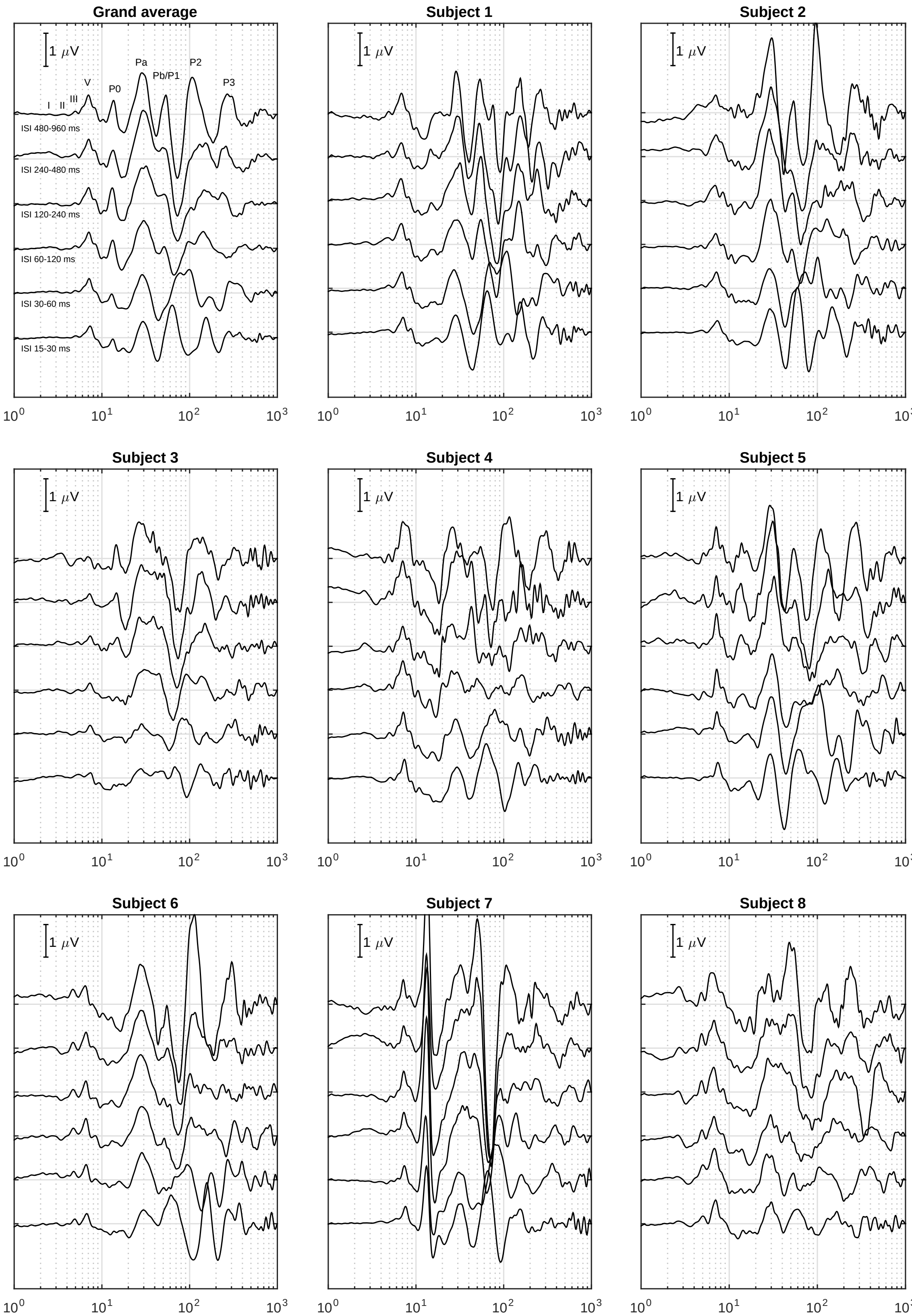

FIG. 4. Grand average and individual AEP responses obtained with the SC-LS_{MD} algorithm at different stimulation rates. The AEP components are labeled in the grand-average response at ISI 480-960 ms. The horizontal and vertical axes correspond, respectively, to latency (in ms) and amplitude. The latency axis has been limited to the range [1-1000] ms.

of the residual error (including a demonstration of the error reduction with respect to the conventional LS deconvolution and with respect to LS-R, i.e. when the LDFDS is applied after the LS deconvolution), and experimental evaluation of the improvement provided by the proposed method, in terms of quality of the estimated AEP responses and computational cost.

Regarding the quality of the estimations, SC-LS significantly improves the LS solution (thanks to the noise removal provided by the latency-dependent filtering). Even though the LS criterion guarantees (under the LS assumptions) that the SC-LS solution is also better than or equal to the LS-R solution, the improvement is moderate in this case (the difference between both solutions is about 31 dB below the response energy, i.e. usually masked by the residual noise), probably because the autocorrelation matrix of the stimulation sequence R_s is close to the identity matrix. Therefore, in practice, the solutions provided by SC-LS and LS-R are very similar.

A relevant difference between SC-LS and LS-R is the requirement that the response in the convolutional model $\mathbf{x}$ belongs to the subspace. In the case of LS-R, if $\mathbf{x}$ is not correctly represented in the subspace (for example, if the response is truncated in order to remove the stimulation artifact), the estimated response does not contain components out of the subspace, but the subspace component is not biased. However, in the case of SC-LS, if $\mathbf{x}$ is not correctly represented in the subspace, the subspace component is biased (due to the transference of energy from the orthogonal complement to the reduced subspace). This effect would be a disadvantage of the proposed method if the reduced representation space was not appropriate to represent the signal involved in the convolution. For this reason, in

SC-LS, an appropriate design of the reduced subspace is critical, in order to appropriately represent the signal involved in the convolution (including both, the biological response and also the stimulation artifact if it was present).

The dimensionality reduction provided by LDFDS (from $J = 14700$ to $J_r = 117$ in the reported experiments) provides several practical advantages for the subspace-constrained deconvolution. The most evident is the reduction of the computational cost associated to the deconvolution, with a reduction of the execution time in a factor 8.5 in the case of the RSLSD algorithm (from 133.7 to 15.6 seconds) and a factor 1.7 in the case of IRSA-120dB (from 27.0 to 15.8 seconds). Additionally, the dimensionality reduction would allow the analysis of the matrix to be inverted (for example, an analysis of its eigenvalues is useful for the estimation of the matrix condition number (Bardy *et al.*, 2014b)), easier as the size of the matrix decreases. Finally, the potential problems associated to matrix inversion (due to low eigenvalues or high condition number of the matrix to be inverted) are alleviated in the reduced representation because the condition number of the matrix to be inverted decreases according to the Cauchy interlacing theorem (the LS deconvolution is better conditioned in the reduced representation space).

In conventional LS deconvolution, the computational cost of IRSA is significantly smaller than that of RSLSD. This advantage disappears when the deconvolution is constrained to the subspace. Two factors contribute to reduce the advantage of IRSA: on one hand, the matrix to be inverted in the subspace is not Toeplitz, and therefore a fast-Fourier-transform-based matrix product is not possible in the reduced representation. On the other hand, part of the advantage of IRSA with respect to RSLSD was associated to the high dimensionality of the matrix to be inverted, and vanishes as the dimensionality decreases. As a consequence, the RSLSD implementation of SC-LS (with a simpler formulation and directly providing the solution at convergence) has a computational cost similar to that of IRSA.

The subspace-constrained least squares deconvolution of overlapping AEPs described in this paper along with the representation of the deconvolved AEPs in the logarithmic time scale enables the comprehensive and uninterrupted visualization of all the AEP components of the auditory pathway (from the cochlea to the cortex). While this type of AEP representation is currently non-standard, we believe that it provides a change of paradigm with potential to become the natural way in which AEPs are represented (both in clinical and research applications) due to the important advantages that it provides relative to the traditional representation of AEPs (in which the ABR, MLR or CAEP components can be only separately visualised). For example, the proposed comprehensive AEP representation would facilitate the exploration of peripheral and central interactions resulting from both bottom-up and top-down processes (Asilador and Llano, 2021; Lesicko and Llano, 2017), or as a possible diagnostic tool for auditory neuropathy spectrum disorder (as this population is characterized by presenting clear cortical but absent brainstem components (Hood, 2007)).

The amplitude reduction observed in the PAMR in Subject 7 as the stimulus rate increased is consistent with the results obntained by Zakaria *et al.* (2019), the only study that to the best of our knowledge has investigated the influence of the stimulus rate on the morphology of the PAMR. Zakaria *et al.* (2019) evaluated three stimulus repetition rates, being 6.1, 11.1 and 17.1 stim/sec; and found that the PAMR threshold increased for the faster repetition rate. In the present study, we show that the PAMR can be reliably recorded at stimulation rates up to 44.4 stim/sec (i.e. ISI 15-30 ms). Future research aimed at characterizing the morphology of the PAMR at faster rates shall benefit from deconvolution algorithms such as the proposed SC-LS.

At group level, the grand-average AEPs and the individual responses show that peripheral components of the response (i.e. from wave I to Pa) can be visually tracked down from the slow to the faster stimulus rates. In contrast, the tracking of central components such as the P1/Pb, P2 and P3 as stimulus rate increases is not straightforward, particularly for ISIs lower than 60-120 ms. Tracking AEP components from a control scenario (in which the neural generators are known) to novel exploratory scenarios (in which the morphology of the responses has not been documented) is an efficient strategy to identify the neural generators of those components (Elberling and Don, 2007). For example, this strategy could be applied to identify AEP components resulting from the analysis of transient AEP responses from binaural stimuli (Martinez *et al.*, 2021) or from ecologically-valid stimuli such as natural speech (Valderrama *et al.*, 2019). The difficulty in tracking central components in the present study could be the result of a suboptimal placement of the active electrode on the head (situated in Fz in this study), as the P1-P2 complex maximizes its magnitude in Cz (Bardy *et al.*, 2014b) and the P3 component in CPz (Hall, 2007). Placing the active electrode far from the neural generator sites may have led to an inefficient characterization of central AEP components, adding an extra difficulty to track these components as a function of the stimulus presentation rate. To this respect, futures studies investigating the morphology of both peripheral and central AEP components at different rates shall benefit from the use of a multi-channel EEG recording setup.

Furthermore, the analysis of the individual AEP waveforms has revealed the existence of the P3 component in all the participants at the slow stimulus rate. This finding was contrary to our expectations, since the P3 component is associated with novelty and expectation, and is typically evoked by stimuli presented at slow rates (e.g. 1 or 0.5 stim/sec) via the oddball paradigm (by comparing the morphology from AEP responses elicited by a deviant stimulus relative to a frequent stimulus (Hall, 2007; Sharma, 2021)). In contrast, the present study uses sequences of a single stimulus (clicks) in which the maximum ISI doubles the minimum ISI. It could be the case that this broad distribution of the ISI induces some degree of novelty on the participant, thus evoking either (i) a consistent P3 component in all the responses of the stimulus sequence, or (ii) a large P3 component only in those responses in which the degree of novelty is higher (probably those with longer ISIs). To respond to this question, a multi-response deconvolution approach would be required to carry out a time-invariant analysis, similar to the one proposed by Valderrama *et al.* (2016).

A potential limitation of the proposed deconvolution method (affecting any deconvolution procedure, also when it is performed in the complete representation space) is the linearity requirement for the least squares criterion. The convolutional method described in equation (1) (or its matrix formulation described in equation (2)) assumes that the auditory system is linear and time invariant (LTI). However, it is well known that auditory evoked responses do not have a linear behavior with the stimulation level (there is a threshold effect, a non linear growing with the stimulation level and a saturation effect (Hall, 2007)) and are not time invariant (the responses changes with the state of the auditory system (Valderrama *et al.*, 2016)). A possible strategy to deal with this limitation consist in the formulation of a multi-response deconvolution with different possible responses associated to different stimulation levels (as proposed in (Martinez *et al.*, 2022)) or to different states of the auditory system (as proposed in (Valderrama *et al.*, 2016)). This way, under a multi-response formulation of the deconvolution, the non-LTI auditory system can be modeled as an LTI-like system. The multi-response deconvolution, necessary for exploring the response of the complete auditory pathway using complex stimulation patterns, would increase the computational requirements dramatically (a preliminary analysis suggests us that the computational cost would increase with the square of the number of responses considered in the multi-response model). Under this new paradigm, the computational optimization proposed in this article is expected to be very relevant.

In summary, the subspace-constrained deconvolution together with the dimensionality reduction provided by LDFDS provide a substantial quality improvement with respect to the conventional LS solution (and very slight improvement with respect to LS-R, being this improvement not very useful in practice), and provides a substantial computational cost reduction with respect to LS or LS-R, particularly important for the estimation of the complete auditory pathway response. The reduction of both the execution time and the dimensionality, together with the inherent flexibility of IRSA or RSLSD, provide new perspectives in the design of evoked potential experiments, with more ecological stimuli, involving the simultaneous deconvolution of multiple responses (associated to multiple categories of acoustical events) and including the response of the complete auditory pathway (Martinez *et al.*, 2021; Valderrama *et al.*, 2019).

ACKNOWLEDGMENTS

This work was partially supported by the Spanish Ministry of Science and Innovation under the project PID2020-119073GB-I00, by Programa Operativo FEDER Andalucía 2014-2020 under the project B.TIC.382.UGR20, and by the Australian Government Department of Health.

[1]See the supplementary materials at [URL will be inserted by AIP] for a PDF file presenting (section 1) the derivation of the least squares solution for an over-determined system of linear equations; (section 2) a description of the effect of an inappropriate subspace selection; (section 3) the mathematical demonstration of the noise reduction provided by the subspace-constrained LS estimation; (section 4) a comparison of subspace-constrained deconvolution vs LDFDS after deconvolution; (section 5) Matlab/Octave functions implementing the LS, LS-R and SC-LS procedures; (section 6) additional experiments with simulations; and (section 7) additional experiments with real EEGs. A compressed directory with examples and MatLab/Octave scripts and functions, aiming to help the reader apply the subspace-constrained LS deconvolution procedure described in this paper is also included in the supplementary materials.

Asilador, A., and Llano, D. A. (**2021**). "Top-down inference in the auditory system: Potential roles for corticofugal projections," Frontiers in Neural Circuits **14**, 1–20.

Bardy, F., Dillon, H., and Dun, B. V. (**2014**a). "Least-squares deconvolution of evoked potentials and sequence optimization for multiple stimuli under low-jitter conditions," Clinical Neurophysiology **125**, 727–737.

Bardy, F., Dun, B. V., Dillon, H., and Cowan, R. (**2014**b). "Least-squares (ls) deconvolution of a series of overlapping cortical auditory evoked potentials: a simulation and experimental study," Journal of Neural Engineering **11**, 046016.

Bardy, F., Dun, B. V., Dillon, H., and McMahon, C. M. (**2014**c). “Deconvolution of overlapping cortical auditory evoked potentials recorded using short stimulus onset-asynchrony ranges,” Clinical Neurophysiology **125**, 814–826.

Bohorquez, J., and Ozdamar, O. (**2006**). “Signal to noise ratio analysis of maximum length sequence deconvolution of overlapping evoked potentials,” Journal of the Acoustical Society of America **119**, 2881–2888.

Burkard, R. F., and Don, M. (**2007**). “The auditory brainstem response,” in *Auditory evoked potentials: basic principles and clinical application*, edited by R. Burkard, M. Don, and J. Eggermont (Lippincott Williams & Wilkins, Baltimore), pp. 229–253.

Burkard, R. F., Finneran, J. J., and Mulsow, J. (**2018**). “Comparison of maximum length sequence and randomized stimulation and averaging methods on the bottlenose dolphin auditory brainstem response,” Journal of the Acoustical Society of America **144**, 308–318.

de la Torre, A., Valderrama, J. T., Segura, J. C., and Alvarez, I. M. (**2019**). “Matrix-based formulation of the iterative randomized stimulation and averaging method for recording evoked potentials,” Journal of the Acoustical Society of America **146**, 4545–4556.

de la Torre, A., Valderrama, J. T., Segura, J. C., and Alvarez, I. M. (**2020**). “Latency-dependent filtering and compact representation of the complete auditory pathway response,” Journal of the Acoustical Society of America **148**, 599–613.

Elberling, C., and Don, M. (**2007**). “Detecting and assessing synchronous neural activity in the temporal domain (snr, response detection),” in *Auditory evoked potentials: basic principles and clinical application*, edited by R. Burkard, M. Don, and J. Eggermont (Lippincott Williams & Wilkins, Baltimore), pp. 102–123.

Eysholdt, U., and Schreiner, C. (**1982**). "Maximum length sequences: A fast method for measuring brain-stem-evoked responses," Audiology **21**, 242–250.

Finneran, J. J., Mulsow, J., and Burkard, R. F. (**2019**). "Signal-to-noise ratio of auditory brainstem responses (abrs) across click rate in the bottlenose dolphin (tursiops truncatus)," Journal of the Acoustical Society of America **145**, 1143–1151.

Gentle, J. E. (**1998**). *Numerical Linear Algebra for Applications in Statistics* (Springer, New York).

Gillespie, P. G., and Muller, U. (**2009**). "Mechanotransduction by hair cells: Models, molecules, and mechanisms," Cell **139**, 33–44.

Goldberger, A., Shenhart, W., and Wilks, S. (**1964**). *Econometric Theory*, Chap. Classical Linear Regression (J. Wiley).

Hall, J. W. (**2007**). *New handbook of auditory evoked potentials*, 58–108 (Pearson Education, Boston).

Hayashi, F. (**2000**). *Econometrics* (Princeton University Press, New Jersey).

Holt, F., and Ozdamar, O. (**2016**). "Effects of rate (0.3-40/s) on simultaneously recorded auditory brainstem, middle and late responses using deconvolution," Clinical Neurophysiology **127**, 1589–1602.

Hood, L. J. (**2007**). "Auditory neuropathy and dys-synchrony," in *Auditory evoked potentials: basic principles and clinical application*, edited by R. Burkard, M. Don, and J. Eggermont (Lippincott Williams & Wilkins, Baltimore), pp. 275–290.

Jewett, D. L., Caplovitz, G., Baird, B., Trumpis, M., Olson, M. P., and Larson-Prior, L. J. (**2004**). "The use of qsd (q-sequence deconvolution) to recover superposed, transient evoked-responses," Clinical Neurophysiology **115**, 2754–2775.

Kohl, M. C., Schebsdat, E., Schneider, E. N., Niehl, A., Strauss, D. J., Ozdamar, O., and Bohorquez, J. (**2019**). "Fast acquisition of full-range auditory event-related potentials using an interleaved deconvolution approach," Journal of the Acoustical Society of America **145**, 540–550.

Lawson, C. L., and Hanson, R. J. (**1974**). Series in Automatic Computation *Solving Least Squares Problems* (Prentice-Hall, Englewood Cliffs, NJ 07632, USA).

Lesicko, A. M. H., and Llano, D. A. (**2017**). "Impact of peripheral hearing loss on top-down auditory processing," Hearing Research **343**, 4–13, doi: https://doi.org/10.1016/j.heares.2016.05.018.

Lütkenhöner, B. (**2010**). "Baseline correction of overlapping event-related responses using a linear deconvolution technique," NeuroImage **52**, 86–96.

Maddox, R. K., and Lee, A. K. C. (**2018**). "Auditory brainstem responses to continuous natural speech in human listeners," eNeuro **5**, e0441, 13p.

Martinez, M., Valderrama, J. T., Alvarez, I., Vargas, J. L., and de la Torre, A. (**2021**). "The transient response to interaural time differences," in *XXVII International Evoked Response Audiometry Study Group (IERASG-2021)*, p. 50.

Martinez, M., Valderrama, J. T., Alvarez, I., Vargas, J. L., and de la Torre, A. (**2022**). "Auditory brainstem responses obtained with randomised stimulation level," International Journal of Audiology **0**, 1–8, https://doi.org/10.1080/14992027.2022.2047233.

Ozdamar, O., and Bohorquez, J. (**2006**). "Signal-to-noise ratio and frequency analysis of continuous loop averaging deconvolution (clad) of overlapping evoked potentials," Journal of the Acoustical Society of America **119**, 429–438.

Press, W. H., Teutolsky, S. A., Vetterling, W. T., and Flannery, B. P. (**2002**). *Numerical Recipes in C: The art of Scientific Computing.*, 2nd ed. (Cambridge University Press, New York).

Sharma, M. (**2021**). “Episode 3: Late-late shows in aepdom - beyond obligatory potentials: When just turning on the same stimulus is not enough,” in *Chapter 8: Cortical Level Testing, in: Basic Concepts of Clinical Electrophysiology*, edited by J. Durrant, C. Fowler, J. Ferraro, and S. Purdy (Plural Publishing, San Diego, CA), pp. 336–348.

Thornton, A. R. D. (**2007**). “Instrumentation and recording parameters,” in *Auditory evoked potentials: basic principles and clinical application*, edited by R. Burkard, M. Don, and J. Eggermont (Lippincott Williams & Wilkins, Baltimore), pp. 73–101.

Thornton, A. R. D., and Coleman, A. (**1975**). “The adaptation of cochlear and brainstem auditory evoked potentials in humans,” Electroencephalograpy and Clinical Neurophysiology **39**, 399–406.

Thornton, A. R. D., and Slaven, A. (**1993**). “Auditory brainstem responses recorded at fast stimulation rates using maximum length sequences,” British Journal of Audiology **27**, 205–210.

Valderrama, J. T., Alvarez, I., de la Torre, A., Segura, J. C., Sainz, M., and Vargas, J. L. (**2012**). “Recording of auditory brainstem response at high stimulation rates using randomized stimulation and averaging,” Journal of the Acoustical Society of America **132**, 3856–3865.

Valderrama, J. T., de la Torre, A., Alvarez, I., Segura, J. C., Sainz, M., and Vargas, J. L. (**2013**). "A portable, modular, and low cost auditory brainstem response recording system including an algorithm for automatic identification of responses suitable for hearing screening," in *Proceedings of the IEEE/EMBS Special Topic Conference on Point-of-Care HealthCare Technologies (PoCHT)*, Bangalore, India, pp. 180–189 (art. no. 6461314).

Valderrama, J. T., de la Torre, A., Alvarez, I., Segura, J. C., Sainz, M., and Vargas, J. L. (**2014**a). "A flexible and inexpensive high-performance auditory evoked response recording system appropriate for research purposes," Biomedical Engineering / Biomedizinische Technik **59**, 447–459.

Valderrama, J. T., de la Torre, A., Alvarez, I., Segura, J. C., Thornton, A. R. D., Sainz, M., and Vargas, J. L. (**2014**b). "Auditory brainstem and middle latency responses recorded at fast rates with randomized stimulation," Journal of the Acoustical Society of America **136**, 3233–3248.

Valderrama, J. T., de la Torre, A., Alvarez, I., Segura, J. C., Thornton, A. R. D., Sainz, M., and Vargas, J. L. (**2014**c). "A study of adaptation mechanisms based on abr recorded at high stimulation rate," Clinical Neurophysiology **125**, 805–813.

Valderrama, J. T., de la Torre, A., and Dun, B. V. (**2018**). "An automatic algorithm for blink-artifact suppression based on iterative template matching: Application to single cannel recording of cortical auditory evoked potentials," Journal of Neural Engineering **15**(016008), 016008, 15p.

Valderrama, J. T., de la Torre, A., Dun, B. V., and Segura, J. C. (**2019**). "Towards the recording of brainstem and cortical evoked potentials from the fine structure of natural speech," in *XXVI International Evoked Response Audiometry Study Group (IERASG) Biennial Symposium*, Sydney, Australia.

Valderrama, J. T., de la Torre, A., Medina, C., Segura, J. C., and Thornton, A. R. D. (**2016**). "Selective processing of auditory evoked responses with iterative-randomized stimulation and averaging: A strategy for evaluating the time-invariant assumption," Hearing Research **333**, 66–76.

Woldorff, M. G. (**1993**). "Distortion of erp averages due to overlap from temporally adjacent erps: Analysis and correction," Psychophysiology **30**, 98–119.

Zakaria, M. N., Abdullah, R., Nik, O., and Nik, A. (**2019**). "The influence of stimulus repetition rate on tone-evoked post-auricular muscle response (pamr) threshold," Ear and Hearing **40(4)**, 1039–1042.